AIAA JOURNAL
Vol. 39, No. 3, March 2001

Parametric Study of Weighted Essentially Nonoscillatory Schemes for Computational Aeroacoustics

San-Yih Lin* and Jeu-Jiun Hu†
National Cheng-Kung University, Tainan 70101, Taiwan, Republic of China

Based on the dissipation and dispersion relations, two groups of weighted essentially nonoscillatory (WENO) schemes are investigated for computational aeroacoustics. For high-order accuracy, all of the WENO schemes are required to be at least fourth-order accurate. Therefore, with a reasonable number of grid points, they can simulate the low-frequency waves with high-order accuracy. Also, for the higher frequency waves, two parameters in the WENO schemes are introduced to reduce their dissipation and dispersion errors. Both upwind and central schemes are considered and compared for order of accuracy and capability of wave capturing. A sequence of numerical simulations is carried out. These test problems are propagation of a sine-wave packet, propagation of a spherical wave, shock and sine wave interactions, and propagation of acoustic, vorticity, and density pulses in a freestream.

I. Introduction

IN developing a numerical scheme of partial differential equations, two standard methods are used. One is the truncated Taylor series method used to derive schemes with high-order accuracy, such as weighted essentially nonoscillatory (WENO),[1,2] compact difference,[3] and 2–4 MacCormack (see Ref. 4) schemes. The other is the Fourier series analysis used to obtain schemes with good quality wave resolution, such as spectral[5] and dispersion-relation-preserving (DRP)[6] schemes. Taylor-type schemes with a reasonable number of grid points can simulate the low-frequency waves with high-order accuracy. From the computational fluid dynamics point of view, Taylor-type schemes with upwind technique[1,2] can capture the discontinuous waves, such as shock waves, very well. However, from the wave propagation point of view, this is not necessarily the best way.[6] On the other hand, Fourier-type schemes can simulate the continuous waves with very high-order resolution. However, most of the Fourier type are central schemes,[1–6] which capture the discontinuous waves with a numerical wiggle. Smoothing techniques must be applied to improve the stability of those schemes. Among Taylor-type schemes, the compact scheme is central and implicit in space; therefore, it can achieve spectral-like resolution[3] and needs some smoothing techniques to stabilize the scheme.

In recent years, considerable progress has been made in the numerical methods for fluid dynamics. Many successful methods employ higher-order upwind interpolations and limiter functions to obtain algorithms possessing high resolution and high stability bounds. The inherently dissipative nature of upwind schemes and limiter functions are beneficial at or near discontinuities. Especially, the implementation of limiter functions makes the schemes more stable for computing solutions with strong shock waves. The WENO scheme is essentially high-order accurate, even in the discontinuous and extreme-point regions. Lockard et al.[7] applied Fourier series analysis to develop high-bandwidth ENO methods with fixed and optimized upwind stencils. Weirs and Candler[8] also used Fourier series analysis to optimize WENO schemes. They developed a symmetric WENO scheme with low dissipation errors. In this paper, we use the original WENO scheme[2] as a basic scheme and apply the Taylor series method and Fourier series analysis to develop the dispersion–dissipation-related WENO schemes. From the preceding two methods, two parameters for controlling dispersion and dissipation errors and two groups of WENO schemes are introduced. One parameter, which is similar to Weirs and Candler's,[8] is obtained from the Fourier series analysis; the other parameter, which is different from Weirs and Candler's, is obtained from controlling the central and upwind weighting. A sequence of numerical simulations are carried out. These test problems are propagation of a sine-wave packet, propagation of a spherical wave, shock and sine wave interactions, and acoustic, vorticity, and density pulses in a freestream.

Received 4 October 1999; revision received 17 May 2000; presented as Paper 2000-2623 at the Fluids 2000 Conference, Denver, CO, 19–22 June 2000; accepted for publication 26 July 2000.

*Professor, Institute of Aeronautics and Astronautics. Member AIAA.
†Graduate Student, Institute of Aeronautics and Astronautics.

II. Numerical Methods

A. Governing Equations

The flows of two-dimensional, compressible, inviscid fluid can be described in conservation form by the Euler equations

$$W_t + F_x + G_y = 0 \tag{1}$$

where $W = (\rho, \rho u, \rho v, \rho e)^T$ and

$$F = \begin{pmatrix} \rho u \\ \rho u^2 + p \\ \rho uv \\ u(\rho e + p) \end{pmatrix}, \qquad G = \begin{pmatrix} \rho v \\ \rho uv \\ \rho v^2 + p \\ v(\rho e + p) \end{pmatrix}$$

where p, ρ, u, v, and e are the pressure, density, x- and y-directional velocity components, and the total energy per unit mass, respectively. The pressure p is given by the equation of state for a perfect gas:

$$p = (\gamma - 1)\left[\rho e - \tfrac{1}{2}\rho(u^2 + v^2)\right] \tag{2}$$

where γ (=1.4 for air) is the ratio of specific heats.

B. Parameters of WENO Schemes

To obtain higher-order accuracy, the parametric studies of the WENO schemes are performed, and two groups of schemes are proposed. First, a formula for a one-dimensional scalar convection equation is introduced. Detailed methodologies about the original WENO scheme may be found in Refs. 1 and 2.

1. *Parameter α_0 Obtained from Fourier Series Analysis*

Consider the approximation of the first derivative $\partial f/\partial x$ at x_l of a uniform grid. Let $f_{l+1/2}$ be an interpolation of f_j, $l-2 \le j \le l+2$:

$$f_{l+\frac{1}{2}} = \tfrac{1}{6}[\alpha_0(2f_{l-2} - 7f_{l-1} + 11f_l) + \alpha_1(-f_{l-1} + 5f_l + 2f_{l+1}) + \alpha_2(2f_l + 5f_{l+1} - f_{l+2})] \tag{3}$$

Then

$$\frac{\partial f}{\partial x}(x_l) = \frac{1}{\Delta x}\left(f_{l+\frac{1}{2}} - f_{l-\frac{1}{2}}\right) \tag{4}$$

The first derivative $\partial f/\partial x$ at x_l is then approximated by

$$\frac{\partial f}{\partial x}(x_l) = \frac{1}{\Delta x}\sum_{j=-3}^{2} a_j f(x_l + j\Delta x) \tag{5}$$

where a_j is a linear combination of α_k, $k = 0, 1, 2$.

The Fourier transform of the left- and right-hand sides of Eq. (5) are

$$i\alpha \tilde{f} \simeq \left(\frac{-i}{\Delta x}\sum_{j=-3}^{2} a_j e^{i\alpha j\Delta x}\right)\tilde{f} \tag{6}$$

where $\tilde{f}$ is the Fourier transform of f.

When the two sides of Eq. (6) are compared, it is clear that the quantity

$$\bar{\alpha} = \frac{-i}{\Delta x}\sum_{j=-3}^{2} a_j e^{i\alpha j\Delta x} \tag{7}$$

is the wave number of the Fourier transform of the finite difference scheme [Eq. (4)]; $\bar{\alpha}\Delta x$ is a periodic function of $\alpha\Delta x$ with period 2π. Here, we combine the truncated Taylor series and Fourier series methods to determine the coefficients, α_0, α_1, and α_2. For the scheme to be fourth-order accurate, the coefficients are required satisfy the following two equalities:

$$\alpha_0 + \alpha_1 + \alpha_2 = 1, \qquad 3\alpha_0 - \alpha_1 + \alpha_2 = 0 \tag{8}$$

In Eq. (8), we choose α_0 as a free parameter. It is desirable to ensure that the Fourier transform of the finite difference is a good approximation to the partial derivative, $\partial f/\partial x$, over the range of wave numbers of interest. Following Tam and Webb,[6] α_0 is chosen to optimize the integrated error E defined as

$$E = \int_0^{\pi} \{\sigma[\mathrm{Re}(\bar{\alpha}\Delta x) - \alpha\Delta x]^2 + (1-\sigma)\{\mathrm{Im}(\overline{\alpha}\Delta x)\}^2\}\, \mathrm{d}(\alpha\Delta x) \tag{9}$$

where σ is a weight on the real part. For a given σ, here α_0 is determined by minimizing the integrated error E. Therefore, α_0 is still used as a free parameter instead of σ. In this paper, four values of α_0 are chosen: 1) fifth-order accuracy, $\alpha_0 = 0.1$; 2) smaller phase error, $\alpha_0 = 0.14$ [$\sigma = 0.155$ in Eq. (9)]; 3) smaller amplitude error, $\alpha_0 = 0.08$ ($\sigma = 0.57$); and 4) optimum phase and amplitude errors, $\alpha_0 = 0.12$ ($\sigma = 0.3$).

For case 1, $\alpha_0 = 0.1$ is determined purely from the Taylor expansion analysis so that the scheme has highest-order accuracy. For case 2, σ is determined to be 0.155 so that the scheme has lower phase error and is close to the DRP scheme[6] (see comment, Sec. II.B.3). Because $\sigma = 0.155$ in Eq. (9), the value of α_0 is obtained to be 0.14 for minimizing E. Based on cases 1 and 2, α_0 is chosen to be 0.08 for the scheme to have smaller amplitude error and α_0 to be 0.12 for the scheme to have optimum phase and amplitude errors. According to Fourier analysis, to have less the $Y\%$ phase error after propagating X wavelengths, one needs

$$\mathrm{Re}(\bar{\alpha}\Delta x - \alpha\Delta x) < (\alpha\Delta x \times Y)/100X \tag{10}$$

Similarly, to obtain less than $Y\%$ amplitude error after propagating X wavelengths, one needs

$$\mathrm{Im}(\bar{\alpha}\Delta x) > \ln[(100 - Y)/100] \times \alpha\Delta x/(2\pi X) \tag{11}$$

Figure 1 shows the phase errors of the partial derivative $\partial f/\partial x$, with 10% phase error ($Y = 10$). For $\alpha_0 = 0.12$, the phase error is less 10% after propagating 100 wavelengths because $\alpha\Delta x$ is up to 1.0 ($\bar{\alpha}_r = \mathrm{Re}\{\bar{\alpha}\}$ and $\bar{\alpha}_i$ is the imaging part). Thus, this upwind finite difference scheme can provide almost no phase error for waves with wavelengths longer than 6.5 mesh spacings. For the fifth-order upwind scheme, $\alpha_0 = 0.1$, the curve starts to deviate from the linear relation $\bar{\alpha}_r = \alpha$ at $\alpha\Delta x = 0.5$. In other words, this upwind scheme will provide larger phase error for waves with wavelengths shorter than 13 mesh spacings. Figure 2 shows the amplitude errors with $Y = 50$. The results of the errors for those schemes are just opposite

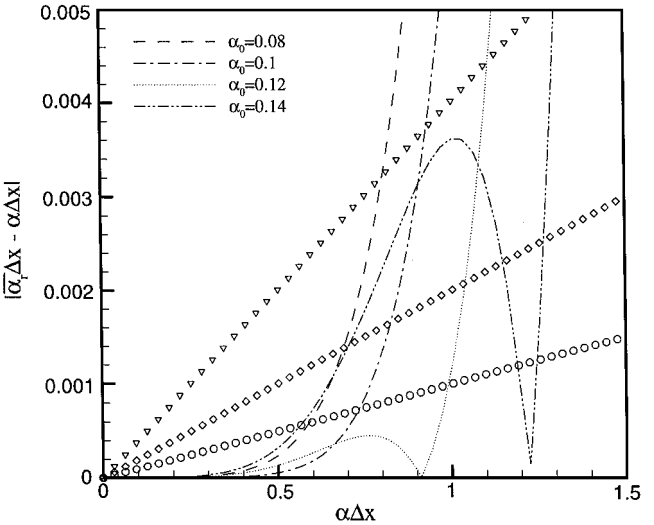

Fig. 1 Phase errors of the partial derivative $\partial f/\partial x$: ∇ = 25 wavelength, $\diamond$ = 50 wavelength, and $\circ$ = 100 wavelength.

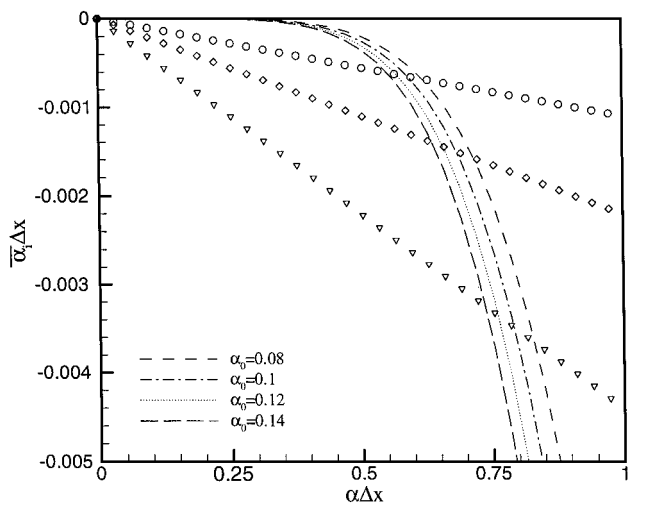

Fig. 2 Amplitude errors of the partial derivative $\partial f/\partial x$: ∇ = 25 wavelength, $\diamond$ = 50 wavelength, and $\circ$ = 100 wavelength.

the results of the phase errors in Fig. 1. Here $\alpha_0 = 0.08$ shows the best result on the amplitude errors. However all of them need at least 10–12 mesh spacings to have lower phase errors.

2. Parameter β Obtained from Controlling Central and Upwind Weighting

Now that the effects of parameter α_0 have been investigated, parameter β is introduced. Consider the one-dimensional scalar convection equation

$$u_t + f(u)_x = 0 \tag{12}$$

The flux is split into two parts as

$$f(u) = f^+(u) + f^-(u) \tag{13}$$

where

$$f^+(u) = 0.5\{f(u) + \beta[\max|f'(u)|]u\}$$
$$f^-(u) = 0.5\{f(u) - \beta[\max|f'(u)|]u\} \tag{14}$$

The maximum is taken over the whole range of u, and β is a nonnegative parameter, $0 \le \beta \le 1$. The scheme is central if $\beta = 0$. If $\beta = 1$ then $\mathrm{d}f^+/\mathrm{d}u \ge 0$ and $\mathrm{d}f^-/\mathrm{d}u \le 0$, and the scheme is fully upwind. For a computed solution with a high gradient or discontinuities, a better choice of β should be used. Following Ref. 9, a scalar function for β is proposed:

$$\beta = \begin{cases} \beta_{\min}, & \text{for} \quad 0 < s < s_1 \\ 1.0, & \text{for} \quad s > s_2 \end{cases} \tag{15}$$

and β is linear between s_1 and s_2. Here $\beta_{\min}$ is less than 1, and

$$s = |u_{i+2} - u_{i+1}| + |u_{i+1} - u_i| + |u_i - u_{i-1}|, \qquad s_1 = M\Delta x_i$$

$$s_2 = \max[(3M+1)\Delta x_i, M\sqrt{\Delta x_i}]$$

where M is a free parameter. The basic idea is that the value of β is chosen to be 1 around the discontinuities and $\beta_{\min}$ in continuous regions. Thus, the scheme can simulate the continuous waves, such as sound waves, at higher-order accuracy and can sharply capture the discontinuous waves, such a shock wave, as most upwind schemes do. For the details of discussion on the values of $\beta_{\min}$ and M, see Ref. 9. In this paper, the values of $\beta_{\min}$ and M are chosen to be 0.1 and 5, respectively.

3. Two Groups of WENO Schemes

Now the WENO schemes are introduced. The numerical flux is expressed as

$$f_{l+\frac{1}{2}} = f^+_{l+\frac{1}{2}} + f^-_{l+\frac{1}{2}} \tag{16}$$

From Eq. (3), a higher-order WENO scheme is given by

$$f^+_{l+\frac{1}{2}} = \tfrac{1}{6}\big[w_0^+\big(2f^+_{l-2} - 7f^+_{l-1} + 11f^+_l\big) + w_1^+\big(-f^+_{l-1} + 5f^+_l + 2f^+_{l+1}\big) + w_2^+\big(2f^+_l + 5f^+_{l+1} - f^+_{l+2}\big)\big] \tag{17}$$

where

$$w_k^+ = \alpha_k^+ \big/ \big(\alpha_0^+ + \alpha_1^+ + \alpha_2^+\big), \qquad k = 0, 1, 2$$

$$\alpha_0^+ = \alpha_0 \big/ \big(\epsilon + S_0^+\big)^2, \qquad \alpha_1^+ = \alpha_1 \big/ \big(\epsilon + S_1^+\big)^2$$

$$\alpha_2^+ = \alpha_2 \big/ \big(\epsilon + S_2^+\big)^2$$

$$S_0^+ = \tfrac{13}{12}\big(f^+_{l-2} - 2f^+_{l-1} + f^+_l\big)^2 + \tfrac{1}{4}\big(f^+_{l-2} - 4f^+_{l-1} + 3f^+_l\big)^2$$

$$S_1^+ = \tfrac{13}{12}\big(f^+_{l-1} - 2f^+_l + f^+_{l+1}\big)^2 + \tfrac{1}{4}\big(f^+_{l-1} - f^+_{l+1}\big)^2$$

$$S_2^+ = \tfrac{13}{12}\big(f^+_l - 2f^+_{l+1} + f^+_{l+2}\big)^2 + \tfrac{1}{4}\big(f^+_{l+2} - 4f^+_{l+1} + 3f^+_l\big)^2 \tag{18}$$

Equation (18) serves as a limiter function,[2] which we will discuss later. The value of ϵ is a small number to avoid the denominator becoming zero.

Here $f^-_{l+1/2}$ is a right-partial upwind interpolation of f_j, $l-1 \le j \le l+3$:

$$f^-_{l+\frac{1}{2}} = \tfrac{1}{6}\big[w_0^-\big(-f^-_{l-1} + 5f^-_l + 2f^-_{l+1}\big) + w_1^-\big(2f^-_l + 5f^-_{l+1} - f^-_{l+2}\big) + w_2^-\big(11f^-_{l+1} - 7f^-_{l+2} + 2f^-_{l+3}\big)\big] \tag{19}$$

where

$$w_k^- = \alpha_k^- \big/ \big(\alpha_0^- + \alpha_1^- + \alpha_2^-\big), \qquad k = 0, 1, 2$$

$$\alpha_0^- = \alpha_0 \big/ \big(\epsilon + S_0^-\big)^2, \qquad \alpha_1^- = \alpha_1 \big/ \big(\epsilon + S_1^-\big)^2$$

$$\alpha_2^- = \alpha_2 \big/ \big(\epsilon + S_2^-\big)^2$$

$$S_0^- = \tfrac{13}{12}\big(f^-_{l-1} - 2f^-_l + f^-_{l+1}\big)^2 + \tfrac{1}{4}\big(f^-_{l-1} - 4f^-_l + 3f^-_{l+1}\big)^2$$

$$S_1^- = \tfrac{13}{12}\big(f^-_l - 2f^-_{l+1} + f^-_{l+2}\big)^2 + \tfrac{1}{4}\big(f^-_l - f^-_{l+2}\big)^2$$

$$S_2^- = \tfrac{13}{12}\big(f^-_{l+1} - 2f^-_{l+2} + f^-_{l+3}\big)^2 + \tfrac{1}{4}\big(f^-_{l+3} - 4f^-_{l+2} + 3f^-_{l+1}\big)^2 \tag{20}$$

Again Eq. (20) serves as a limiter function. If one sets $S_0^\pm = S_1^\pm = S_2^\pm = 0$, we say the finite difference is without a limiter function. In this case, $w_k^\pm = \alpha_k$, $k = 1, 2, 3$.

Two parameters, α_0 and β, have been introduced. The main work of this paper is to study their effects on the order of accuracy and the capability of wave capturing. To minimize the effect of time integration, the following fourth-order Runge–Kutta time integration scheme is used:

$$\frac{dw}{dt} = L(w), \qquad w^{(1)} = w^n + \tfrac{1}{2}\Delta t L(w^n)$$

$$w^{(2)} = w^n + \tfrac{1}{2}\Delta t L\big(w^{(1)}\big), \qquad w^{(3)} = w^n + \tfrac{1}{2}\Delta t L\big(w^{(2)}\big)$$

$$w^{n+1} = \tfrac{1}{3}\big(-w^n + w^{(1)} + 2w^{(2)} + w^{(3)} + \tfrac{1}{6}\Delta t L\big(w^{(3)}\big)\big) \tag{21}$$

where $L(w)$ is the spatial discretization operator given by Eq. (4).

When the two preceding parameters, α_0 and β, are used, two groups of WENO schemes, WENO-X and WENO-Y, are introduced. We use WENO-C-Y to represent the central-type scheme, that is, $\beta = 0$ in Eq. (14), WENO-U-Y to represent the fully upwind scheme with $\beta = 1$, and WENO-B-Y to represent the partially upwind scheme with the proposed β function [Eq. (15)]. From Fourier analysis, the central-type schemes (WENO-C-Y) have no amplitude error (because $\partial f^+/\partial x$ and $\partial f^-/\partial x$ have the same amount of amplitude error with different signs) and the same phase error as the data in Fig. 1. WENO-X-T represents the fifth-order scheme with $\alpha_0 = 0.1$, WENO-X-A the smaller amplitude error scheme with $\alpha_0 = 0.08$, WENO-X-D the optimum phase-amplitude error scheme with $\alpha_0 = 0.12$, and WENO-X-P the smaller phase error scheme with $\alpha_0 = 0.14$. Also, we use a linear (nonlinear) WENO scheme to represent the WENO scheme without (with) the limit function, Eqs. (18) and (20), respectively. Note that the nonlinear WENO-U-T scheme is the original WENO scheme,[2] the linear WENO-C-T scheme is the standard sixth-order central scheme, and the linear WENO-C-P scheme is close to the DRP scheme.[6] To demonstrate the performance of the proposed schemes, studies on the order of accuracy and the capability of wave capturing of those schemes were carried out.

III. Accuracy of WENO Schemes

In this section, the accuracy of linear WENO schemes are studied for the linear equation

$$u_t + u_x = 0, \qquad -1 \le x \le 1$$

$$u(x, 0) = u_0(x), \qquad \text{periodic}$$

In Table 1, we show errors of four linear WENO-U-X schemes at $t = 1$ for the initial condition $u_0(x) = \sin(\pi x)$. N is the number of grid points. One can see that WENO-U-T has fifth-order accuracy and is the best among the four schemes. The rest of the schemes have fourth-order accuracy, and WENO-U-D is the best among those three schemes. Because this example is a simple sine-wave propagation problem, central schemes will produce better results than upwind schemes do. Table 2 shows errors of the four linear WENO-C-X schemes. Again, WENO-C-T is the best and has about sixth-order accuracy. From here, for the lower-frequency case, Taylor series analysis can give a good estimate on the order of accuracy.

Table 3 shows the errors of four linear WENO-U-X schemes at $t = 1$ for the initial condition $u_0(x) = \sin(n\pi x)$, $n = 1$–8. In this case, the number of grid points N is fixed to be 40. For fixed n and N, we compare the error of each scheme for a fixed and determine which scheme is better in the higher-frequency computations. One can see that, for $n = 6$ and 8, all of the schemes give larger errors. This indicates that, for a higher-frequency case, upwind schemes need more grid points in each period. Table 4 shows the errors of four linear WENO-C-X schemes. It shows that WENO-C-D gives good resolution at n up to 6. In other words, the WENO-C-D scheme can provide adequate approximation to waves with wavelengths longer

Table 1 Order of accuracy of the four WENO-U-X schemes without limiters at $t = 1$ for the initial condition $u_0(x) = \sin(\pi x)$

N	L_∞	Order	L_1	Order
		WENO-U-P		
10	7.5×10^{-3}	——	5.3×10^{-3}	——
20	4.3×10^{-4}	4.1	3.0×10^{-4}	4.2
40	2.6×10^{-5}	4.1	1.7×10^{-5}	4.1
80	1.6×10^{-6}	4.0	1.0×10^{-6}	4.0
		WENO-U-D		
10	5.8×10^{-3}	——	3.7×10^{-3}	——
20	2.5×10^{-4}	4.5	1.6×10^{-4}	4.5
40	1.3×10^{-5}	4.2	8.4×10^{-6}	4.3
80	7.9×10^{-7}	4.1	4.1×10^{-7}	4.2
		WENO-U-T		
10	4.9×10^{-3}	——	3.1×10^{-3}	——
20	1.6×10^{-4}	5.0	1.0×10^{-4}	5.0
40	5.0×10^{-6}	5.0	3.2×10^{-6}	5.0
80	1.5×10^{-7}	5.0	1.0×10^{-7}	5.0
		WENO-U-A		
10	5.6×10^{-3}	——	3.6×10^{-3}	——
20	2.6×10^{-4}	4.4	1.6×10^{-4}	4.5
40	1.4×10^{-5}	4.2	9.0×10^{-6}	4.2
80	8.1×10^{-7}	4.1	5.2×10^{-7}	4.1

Table 2 Order of accuracy of the four WENO-C-X schemes without limiters

N	L_∞	Order	L_1	Order
		WENO-C-P		
10	4.4×10^{-3}	——	3.3×10^{-3}	——
20	3.7×10^{-4}	3.6	2.5×10^{-4}	3.7
40	2.5×10^{-5}	3.9	1.6×10^{-5}	4.0
80	1.6×10^{-6}	4.0	1.0×10^{-6}	4.0
		WENO-C-D		
10	1.6×10^{-3}	——	1.2×10^{-3}	——
20	1.8×10^{-4}	3.2	1.2×10^{-4}	3.3
40	1.2×10^{-5}	3.8	8.1×10^{-6}	3.9
80	7.9×10^{-7}	4.0	5.1×10^{-7}	4.0
		WENO-C-T		
10	1.4×10^{-3}	——	1.0×10^{-3}	——
20	2.1×10^{-5}	6.0	1.4×10^{-5}	6.2
40	3.4×10^{-7}	6.0	2.2×10^{-7}	6.0
80	5.7×10^{-9}	5.9	3.4×10^{-9}	6.0
		WENO-C-A		
10	4.1×10^{-3}	——	3.0×10^{-3}	——
20	2.2×10^{-4}	4.2	1.5×10^{-4}	4.4
40	1.3×10^{-5}	4.1	8.6×10^{-6}	4.1
80	8.0×10^{-7}	4.0	5.2×10^{-7}	4.0

than 6.5 mesh spacings. From Tables 3 and 4, among the four central WENO schemes, WENO-C-T and WENO-C-D schemes give better approximations for a lower-frequency case, and WENO-C-D and WENO-C-P schemes gives better approximations for a higher-frequency case. Moreover, the WENO-C-P gives better results for $n = 8$ than for $n = 6$. This phenomenon is consistent with the data of Fig. 1, which shows that WENO-C-P gives lower phase error at $n = 8$ than at $n = 6$.

IV. Numerical Results

A. Propagation of a Sine-Wave Packet

Consider the one-dimensional linear equation[10]

$$u_t + u_x = 0, \qquad 0 \le x \le 3, \qquad t > 0$$

The initial condition is a sine-wave packet modulated by a Gaussian centered at $x = \frac{1}{2}$:

$$u(x, 0) = \exp\left[-16\left(x - \tfrac{1}{2}\right)^2\right] \sin(40\pi x)$$

Table 3 Order of accuracy of the four WENO-U-X schemes without limiters for the initial condition $u_0(x) = \sin(n\pi x)$

n	L_∞	L_1
	WENO-U-P	
1	2.6×10^{-5}	1.7×10^{-5}
2	8.6×10^{-4}	5.7×10^{-4}
4	2.9×10^{-2}	2.0×10^{-2}
6	0.24	0.15
8	0.68	0.44
	WENO-U-D	
1	1.3×10^{-5}	8.4×10^{-6}
2	5.0×10^{-4}	3.2×10^{-4}
4	2.3×10^{-2}	1.5×10^{-2}
6	0.20	0.13
8	0.66	0.43
	WENO-U-T	
1	5.1×10^{-6}	3.2×10^{-6}
2	3.2×10^{-4}	2.0×10^{-4}
4	1.9×10^{-2}	1.2×10^{-2}
6	0.19	0.12
8	0.68	0.44
	WENO-U-A	
1	1.4×10^{-5}	9.0×10^{-6}
2	5.1×10^{-4}	3.3×10^{-4}
4	2.2×10^{-2}	1.4×10^{-2}
6	0.20	0.13
8	0.72	0.47

Table 4 Order of accuracy of the four WENO-C-X schemes without limiters

n	L_∞	L_1
	WENO-C-P	
1	2.5×10^{-5}	1.6×10^{-5}
2	7.5×10^{-4}	4.9×10^{-4}
4	1.8×10^{-2}	1.2×10^{-2}
6	6.7×10^{-2}	4.9×10^{-2}
8	3.5×10^{-2}	2.4×10^{-2}
	WENO-C-D	
1	1.2×10^{-5}	8.1×10^{-6}
2	4.2×10^{-4}	2.3×10^{-4}
4	6.3×10^{-3}	4.2×10^{-3}
6	6.1×10^{-3}	4.0×10^{-3}
8	0.27	0.18
	WENO-C-T	
1	3.4×10^{-7}	2.2×10^{-7}
2	4.2×10^{-5}	2.8×10^{-5}
4	5.1×10^{-3}	3.4×10^{-3}
6	7.9×10^{-2}	5.2×10^{-2}
8	0.50	0.33
	WENO-A	
1	1.3×10^{-5}	8.6×10^{-6}
2	4.4×10^{-4}	2.9×10^{-4}
4	1.6×10^{-2}	1.1×10^{-2}
6	0.15	0.10
8	0.72	0.48

First, a mesh of size $\Delta x = \frac{1}{160}$ and Courant–Friedrichs–Lewy number (CFL) = 0.4 are used. Figure 3 shows the numerical results obtained by the linear WENO schemes at time $t = 2$. Figure 3c shows that the WENO-C-D scheme gives almost no amplitude and phase errors. Although the WENO-C-A scheme gives no amplitude error, it has time delay. With the same grid, the WENO-U-X schemes produce large amplitude errors. For this example, the WENO-U-X schemes need a mesh of size about $\Delta x = \frac{1}{320}$ to produce resolution similar to WENO-C-X schemes. Figure 4 shows the numerical results obtained by the linear WENO-U-X schemes. With such a grid, the four schemes give almost no phase errors. It means that, for a pure sine-wave propagation, one shall use central schemes instead of upwind schemes.

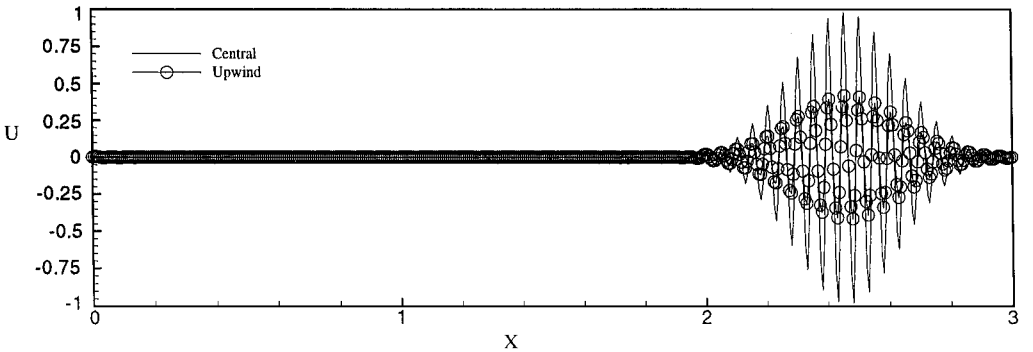

a) WENO-X-A

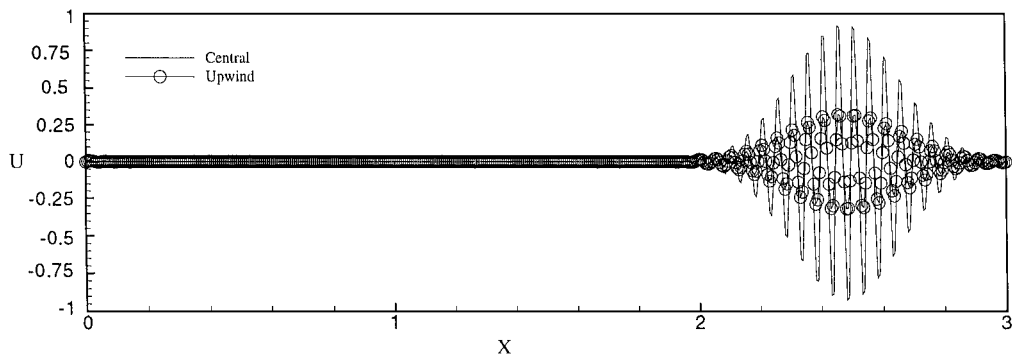

b) WENO-X-T

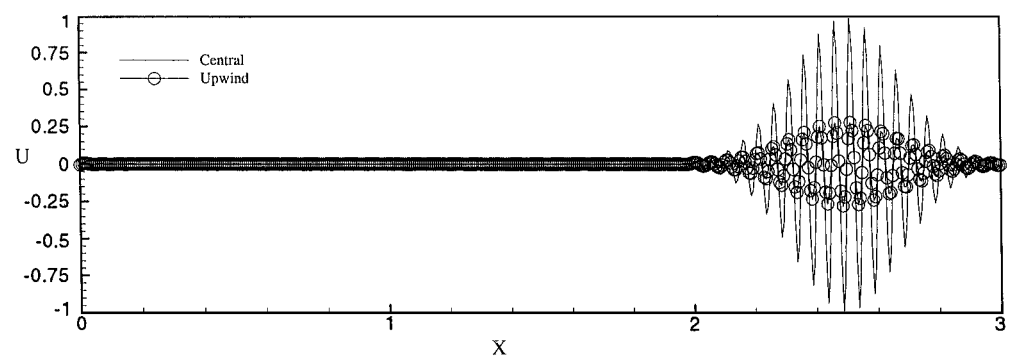

c) WENO-X-D

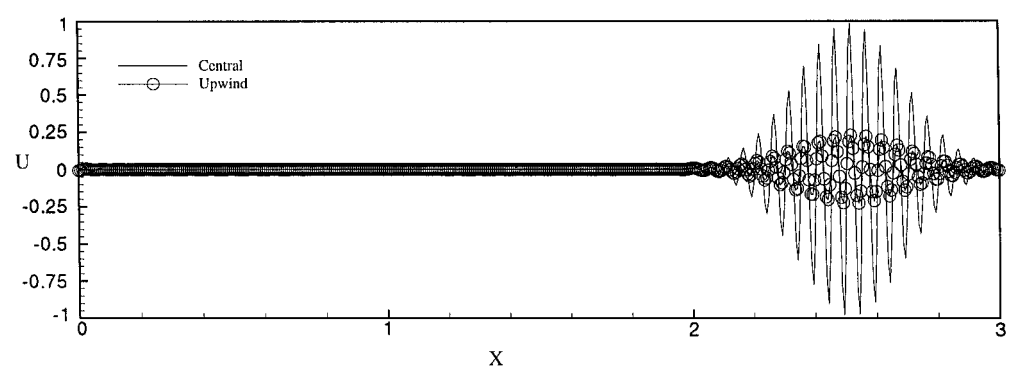

d) WENO-X-P

Fig. 3 Numerical results obtained by linear WENO schemes.

B. Propagation of a Spherical Wave

Consider the spherical wave equation[11]

$$u_t + u_x + u/r = 0, \qquad 5 \le x \le 450, \qquad t > 0$$

solved for the conditions

$$u(x, 0) = 0$$

$$u(5, t) = \sin[(\pi/4)t]$$

The computed results obtained by four linear WENO-C-X schemes at $t = 400$ with $\Delta x = 1$ and $\Delta t = 0.5$ are shown in Fig. 5. Overall, there is good agreement between the numerical data and the exact solution. Near the wavefront in Fig. 5b, the agreement is not as good due to dissipation, dispersion, and a sharp front effect. The WENO-C-P scheme obtains the smallest dissipation error with larger dispersion error and wiggle at the wave front. On the other hand, the WENO-C-D gives the optimum solution. Figure 6 shows the computed results obtained by four WENO-U-X schemes. For $x \le 40$, four upwind schemes give good agreement with the exact solution as shown in Fig. 6a. However, there are large dissipation errors at the wave front. From Secs. VI.A and VI.B, we conclude that the WENO-X-D schemes give better results. For the following

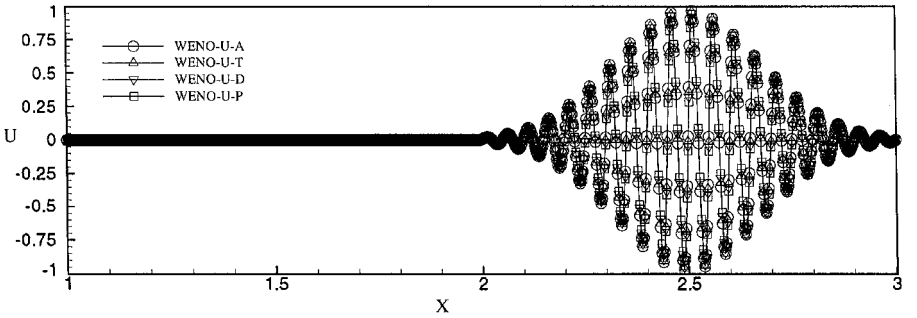

Fig. 4 Numerical results obtained by the WENO-U-X schemes with finer grid system.

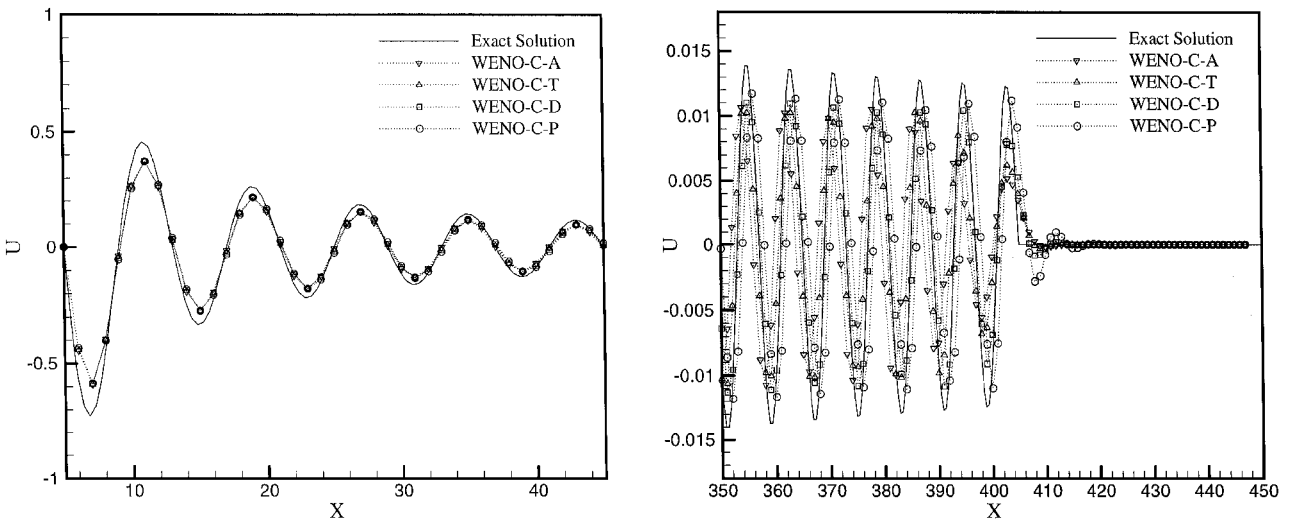

a) $5 \le x \le 40$ **b) $350 \le x \le 450$**

Fig. 5 Computed results obtained by four WENO-C-X schemes at $t = 400$ with $\Delta x = 1$ and $\Delta t = 0.5$.

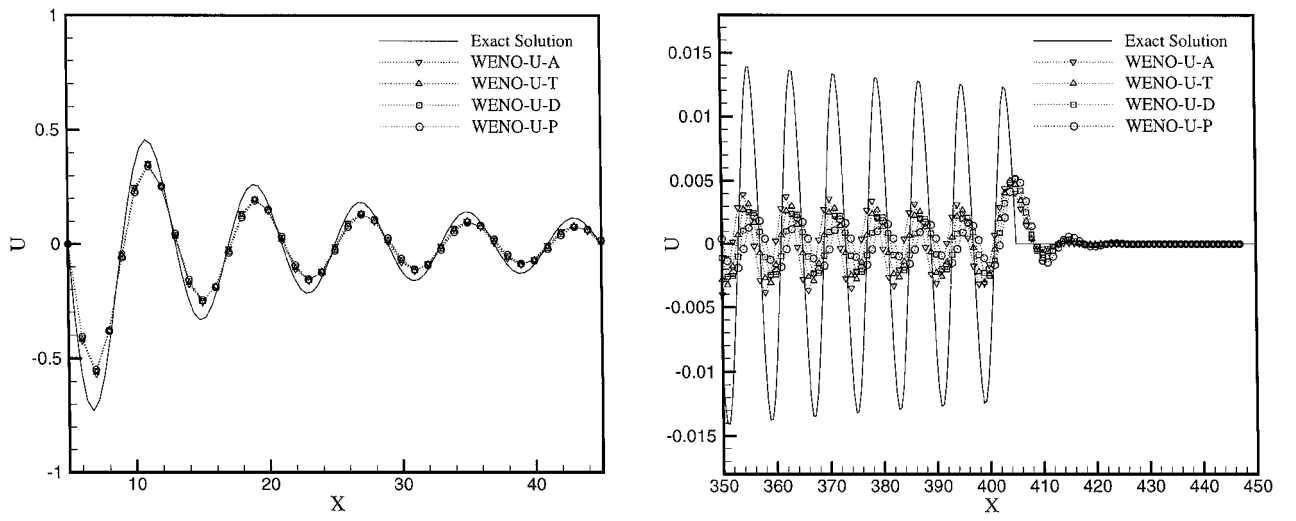

a) $5 \le x \le 40$ **b) $350 \le x \le 450$**

Fig. 6 Computed results obtained by four WENO-U-X schemes.

two examples, because they are nonlinear, the nonlinear WENO schemes and the WENO-B-Y scheme are investigated.

C. Shock and Sine Wave Interactions

The governing equations are the one-dimensional Euler equations with the initial condition

$$(\rho, q, p)_L = (3.85714, 2.62936, 10.33333), \qquad x < -4$$

$$(\rho, q, p)_R = [1 + 0.2\sin(5x), 0.0, 1.0], \qquad x \ge -4$$

where ρ, q, and p are density, velocity, and pressure, respectively. This example contains both shocks and fine structures in smooth regions, a simple model for shock–turbulence interactions.[12] The computational domain is $[-5, 5]$, and a mesh of size $\Delta x = \frac{1}{40}$ is used. Figure 7 shows the density and pressure distribution at time $t = 1.8$ obtained by four nonlinear WENO-U-X schemes. The solid line is obtained with a 2000 grid point scheme and can be regarded as an exact solution. Because this example contains both continuous and discontinuous waves, the computed solution of the WENO-C-D scheme blows up around $t = 0.332$. From this result, one can see that the condition, $\mathrm{d}f^+/\mathrm{d}u \ge 0$ and $\mathrm{d}f^-/\mathrm{d}u \le 0$, is important for the strong discontinuous computations. For the nonlinear WENO-C-D scheme, because $f^+ = f^- = f$, the scheme cannot ensure that the

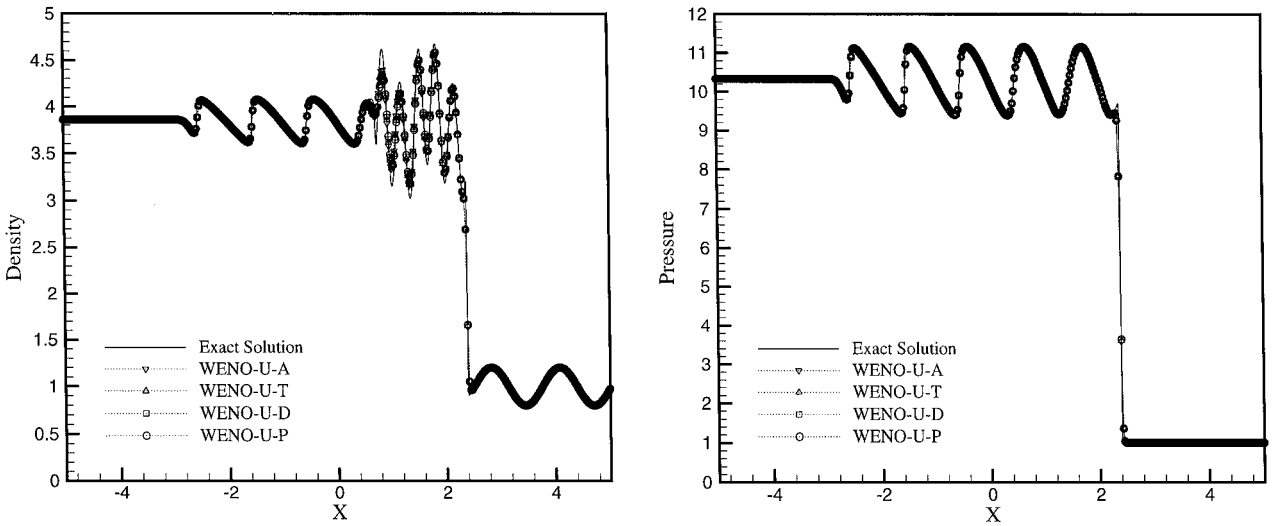

Density **Pressure distribution**

Fig. 7 Four nonlinear WENO-U-X schemes results obtained at time $t = 1.8$.

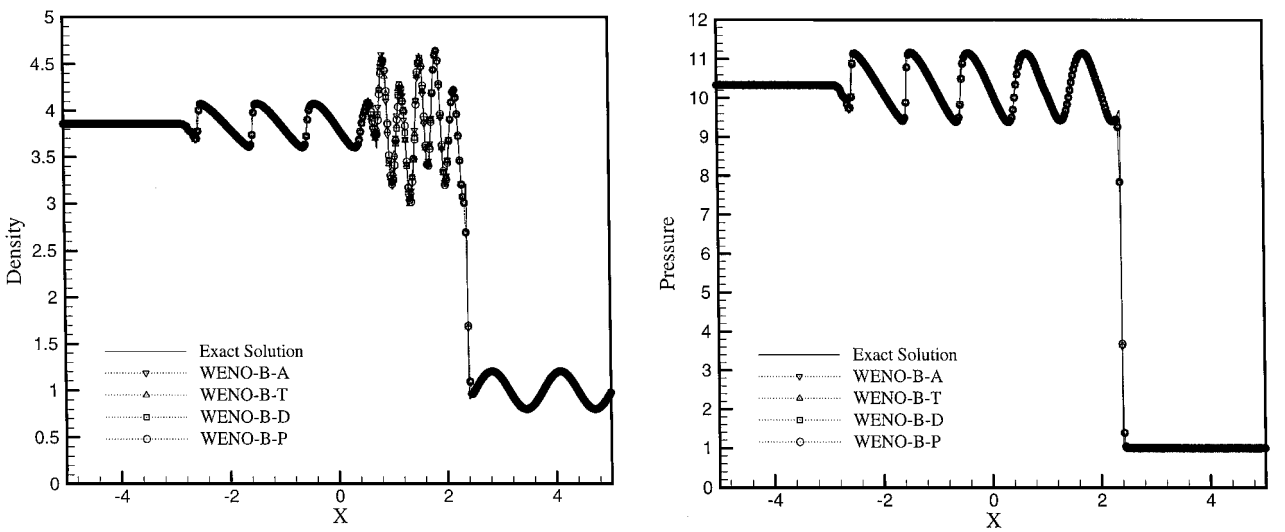

Density **Pressure distribution**

Fig. 8 Nonlinear WENO-B-D scheme results obtained at time $t = 1.8$.

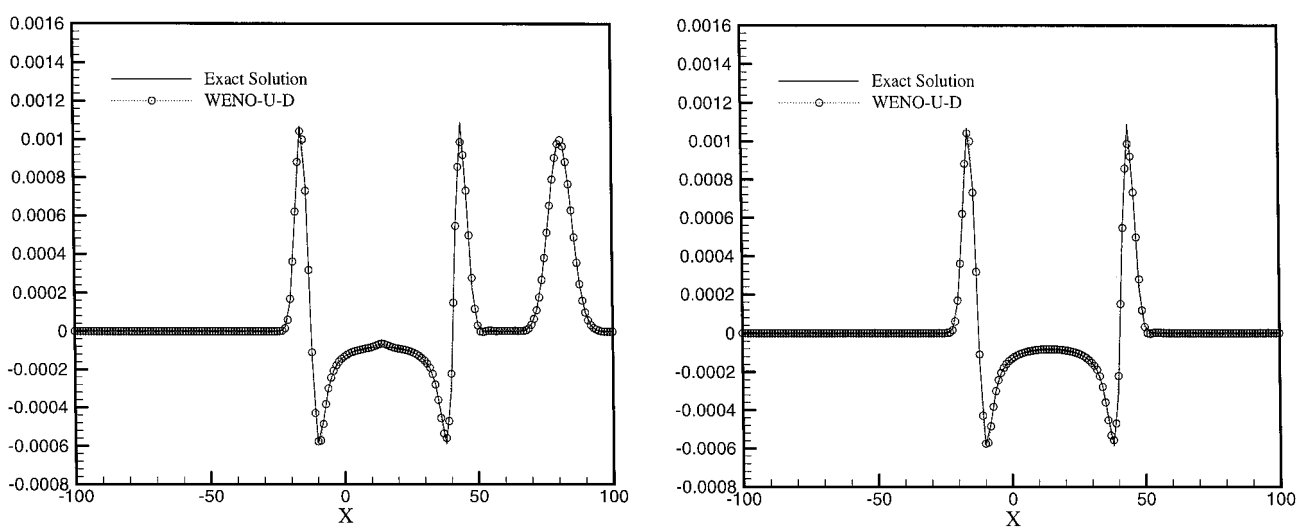

Density **Pressure distribution**

Fig. 9 Nonlinear WENO-U-D scheme results obtained along $y = 0.0$ at $T = 28.45$.

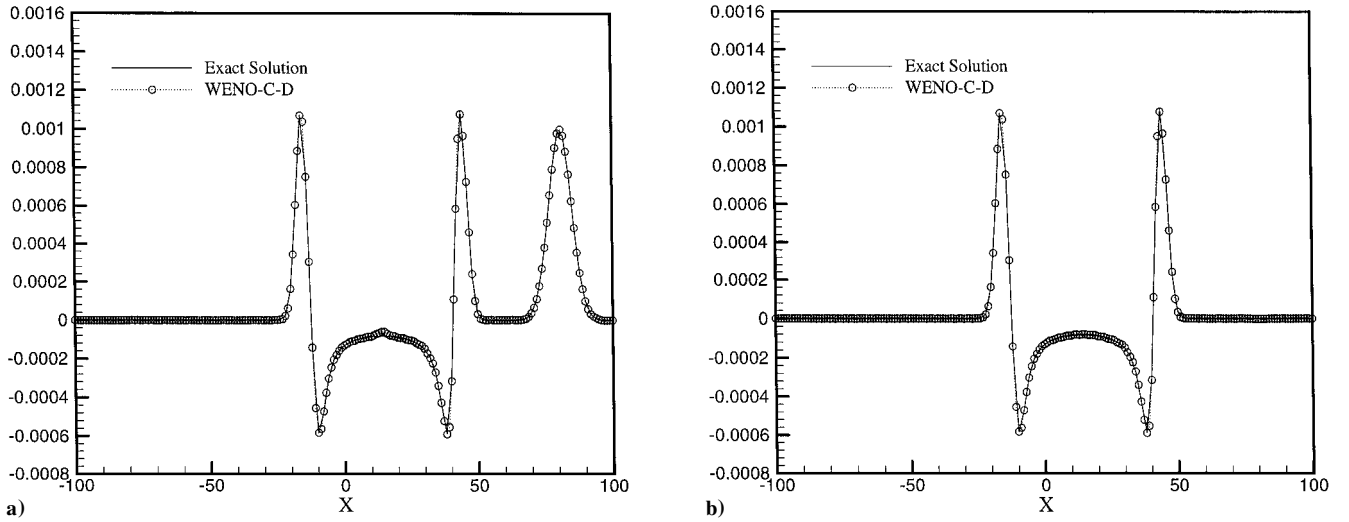

Fig. 10 Nonlinear WENO-C-D scheme results for a) density and b) pressure disturbance.

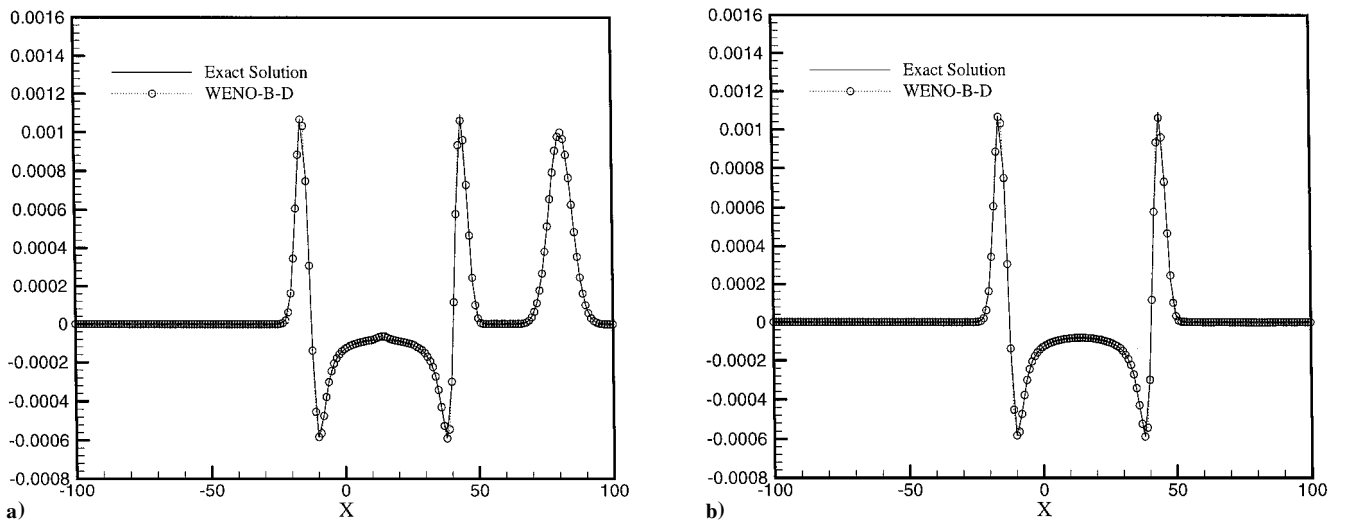

Fig. 11 Nonlinear WENO-B-D scheme results for a) density and b) pressure disturbance.

condition is satisfied for a general function f. Figure 8 shows the density and pressure distribution obtained by the nonlinear WENO-B-Y schemes. The results are better than those obtained by nonlinear WENO-U-Y schemes.

D. Propagation of Acoustic, Vorticity, and Density Pulses in a Freestream

To examine the effectiveness of the WENO scheme for simulating the acoustic wave, the acoustic, vorticity, and density pulses in a freestream of $M_\infty = 0.5$ are tested. From the preceding three examples, the WENO-X-D schemes have better performance than the others. In this example, only the WENO-X-D schemes are investigated. The initial conditions and time for this test are the same as those of Tam and Webb.[6] The disturbance pulses are released at $T = 0$ and are relatively small so that the nonlinear numerical solutions may be compared with the exact solutions of the linearized Euler equations. The computation domain is $[-100, 100]^2$ and is uniformly divided into a 200×200 grid system. Figure 9 shows the density and pressure disturbance along $y = 0.0$ at $T = 28.45$ obtained by the nonlinear WENO-U-D scheme. The computational results compare well with the analytic data. Figure 10 shows the computational solutions obtained by the nonlinear WENO-C-D scheme. The results are good, although a minor wiggle appears from $x = 0$ to 30. Figure 11 shows the computational solutions obtained by the nonlinear WENO-B-D scheme. Again the results are better than those obtained by nonlinear WENO-U-D and WENO-C-D schemes.

V. Conclusions

With the use of the Taylor series and Fourier series methods, WENO schemes are investigated, and two parameters in the WENO schemes are proposed. One parameter is used to control the central- or upwind-type scheme; the other one is used to optimize dissipation and dispersion errors of the schemes. For a low-frequency wave solution, the standard sixth-order central scheme, linear WENO-C-T, gives a good numerical result. However, for a high-frequency wave solution, one should use central schemes with lower dissipation and dispersion errors, such as the WENO-C-D and WENO-C-P schemes. Moreover, for a high-frequency wave solution with small discontinuities, such as the propagation of a spherical wave, the numerical results indicated that the WENO-C-D scheme gives the best results among all of WENO schemes. On the other hand, for solving a solution with strong discontinuities, the nonlinear WENO-B-D scheme is recommended.

Acknowledgments

This work was partially supported by the National Science Council of the Republic of China under Contracts NSC 89-2212-E-006-005. The authors also thank C. W. Shu and G. S. Jiang, who provided the code of the original WENO scheme.

References

[1]Liu, X. D., Osher, S., and Chan, T., "Weighted Essentially Non-Oscillatory Schemes," *Journal of Computational Physics*, Vol. 115, No. 1, 1994, pp. 200–212.

[2]Jiang, G. S., and Shu, C. W., "Efficient Implementation of Weighted ENO Schemes," *Journal of Computational Physics*, Vol. 126, No. 1, 1996, pp. 202–228.

[3]Lele, S. K., "Compact Finite Difference Schemes with Spectral-Like Resolution," *Journal of Computational Physics*, Vol. 103, No. 1, 1992, pp. 16–42.

[4]Gottlieb, D., and Turkel, E., "Dissipative Two-Four Methods for Time-Dependent Problems," *Mathematics of Computation*, Vol. 30, No. 136, 1976, pp. 703–723.

[5]Gottlieb, D., and Orszag, S. A., *Numerical Analysis of Spectral Methods*, Society for Industrial and Applied Mathematics, Philadelphia, 1977, Secs. 2 and 11.

[6]Tam, C. K. W., and Webb, J. C., "Dispersion-Relation-Preserving Finite Difference Schemes for Computational Acoustics," *Journal of Computational Physics*, Vol. 107, No. 2, 1993, pp. 262–281.

[7]Lockard, D. P., Brentner K. S., and Atkins, H. L., "High-Accuracy Algorithms for Computational Aeroacoustics," *AIAA Journal*, Vol. 33, No. 2, 1995, pp. 246–251.

[8]Weirs, V. G., and Candler, G. V., "Optimization of Weighted ENO Schemes for DNS of Compressible Turbulence," AIAA Paper 97-1940, July 1997.

[9]Lin, S. Y., and Chen, Y. F., "Numerical Study of MUSCL Schemes for Computational Aeroacoustics," AIAA Paper 97-0023, Jan. 1997.

[10]Trefethen, L. N., "Group Velocity in Finite Difference Schemes," *SIAM Review*, Vol. 24, No. 2, 1982, pp. 113–135.

[11]Tam, C. K. W., "Benchmark Problems and Solutions," *ICASE/LaRC Workshop on Benchmark Problems in Computational Aeroacoustics*, edited by J. C. Hardin, J. R. Ristorcelli, and C. K. W. Tam, NASA CP-3300, 1995, pp. 1–14.

[12]Cockburn, B., Lin, S. Y., and Shu, C. W., "TVB Runge–Kutta Local Projection Discontinuous Galerkin Finite Element Method for Conservation Laws III: One Dimensional Systems," *Journal of Computational Physics*, Vol. 84, No. 1, 1989, pp. 90–113.

P. J. Morris
Associate Editor